Vol. 90: 121–139, 2024
https://doi.org/10.3354/ame02012

AQUATIC MICROBIAL ECOLOGY
Aquat Microb Ecol

Published September 12

Shore and mid-channel surveys reveal distinct phytoplankton–bacterial population associations along an urban estuary

Georgie E. Humphries[1,2,3], Mariapaola Ambrosone[1], Zabdiel Roldan-Ayala[1,2,4], Maximillian Brown[1,2], Dianne I. Greenfield[1,2,3,*]

[1]Advanced Science Research Center at the Graduate Center, City University of New York, New York, NY 10031, USA
[2]School of Earth and Environmental Sciences, Queens College, City University of New York, Flushing, NY 11367, USA
[3]Earth and Environmental Sciences, Graduate Center, City University of New York, New York, NY 10016, USA

[4]*Present address:* Virginia Institute of Marine Science, College of William & Mary, Gloucester Point, VA 23062, USA

ABSTRACT: A growing body of literature has highlighted the importance of phytoplankton–bacterial associations to marine and estuarine ecological and biogeochemical function, but their population linkages remain sparsely characterized within urban estuaries. Since many developed coastlines are heavily impacted by anthropogenic nutrient inputs, elucidating their phytoplankton–bacterial dynamics provides insight into nutrient cycling, productivity, and can help inform water quality management. This study compared surface (0.5 m depth) physical water quality, cell abundances of major phytoplankton taxa and bacteria, as well as concentrations of chlorophyll *a* (chl *a*) and dissolved organic matter (DOM) in the nitrogen (N)-enriched Western Long Island Sound (WLIS), USA, between mid-channel and shore sites (in 2020 and 2021). Shore bacterial and phytoplankton abundances as well as DOM concentrations (primarily dissolved organic N and carbon [DOC]), were significantly higher than mid-channel, especially during summer, indicative of terrestrial loading influencing microbial assemblages as well as N and C cycling. Abundances of key phytoplankton taxa were better indicators of bacterial abundances than chl *a*, as bacterial abundances positively and significantly correlated with those of dinoflagellates, especially the most common genera *Prorocentrum* (mid-channel, shore) and *Heterocapsa* (shore only), but not with diatoms. However, pennate diatom abundances negatively and significantly correlated with DOC concentrations in the mid-channel. Results highlight the impact of terrestrial inputs on WLIS microbial assemblage dynamics, presumably by favoring bacteria and dinoflagellate population coupling, as well as shed new ecological insight into how phytoplankton and bacterial communities respond to nutrient loadings in urban estuaries.

KEY WORDS: Algal–bacterial interactions · Dissolved organic matter · Dinoflagellates · DOC · Nitrogen · Long Island Sound · Diatoms · *Prorocentrum*

1. INTRODUCTION

A growing body of literature has shown that marine and estuarine phytoplankton–bacterial community associations are vital to ecological and biogeochemical function. For example, field and modeling studies have identified several mechanisms by which phytoplankton cells generate organic matter (OM). This includes the exudation of nutrients into the surrounding microscale environment (Bell & Mitchell 1972, Seymour et al. 2017) and cell lysis releasing dissolved organic matter (DOM), composed of dissolved orga-

*Corresponding author: dgreenfield@gc.cuny.edu

nic nitrogen, phosphorus, and carbon (DON, DOP, and DOC, respectively) (Suttle 2005). These components provide essential bioactive compounds to bacterial communities that may increase their populations (Larsson & Hagström 1979, Ducklow 2000, Keller & Hood 2011, Fu et al. 2020, Variem & Kizhakkedath 2021). Similarly, bacterial community composition and cell numbers often track phytoplankton abundances (Riemann et al. 2000, Morán et al. 2013, Klindworth et al. 2014, Sison-Mangus et al. 2016, Kirchman et al. 2017) and could affect the rates and mechanisms by which major nutrients (N, C, and others) are cycled. Field and laboratory studies have shown that some phytoplankton taxa (including dinoflagellates and diatoms) contribute more DOC and DON to the bulk DOM pool than other taxa, driving inter-annual variability in bacterial community composition, particularly under nutrient-enriched conditions (Bird & Karl 1999, Riemann et al. 2000, Arrieta & Herndl 2002, Arandia-Gorostidi et al. 2022). Conversely, bacterial communities can produce exogenous organic and inorganic compounds necessary for phytoplankton growth and metabolism, such as vitamins (Haines & Guillard 1974, Amin et al. 2012, Sañudo-Wilhelmy et al. 2014). These examples illustrate the wide-ranging and intricate ecological connections that exist between phytoplankton and bacterial communities.

Developed coastlines are especially vulnerable to anthropogenic nutrient loading and frequently have elevated abundances of both phytoplankton and bacteria relative to undeveloped coastlines (Heisler et al. 2008, Verity & Borkman 2010, Li et al. 2014, Reed et al. 2015). Eutrophication can further fuel autochthonous DOM production in estuaries (Asmala et al. 2018), increasing heterotrophic microbial abundances. Yet the ecological relationships between phytoplankton and bacterial populations remain sparsely characterized in urban estuaries, hindering our capacity to understand the associated biogeochemical processes.

Several laboratory and field studies have indicated that certain phytoplankton taxa have strong physiological and ecological connections with bacterial population levels (e.g. Grossart et al. 2005, Sison-Mangus et al. 2014). For example, in the urbanized Delaware Estuary, USA, numbers of dinoflagellates, haptophytes, and prasinophytes were more significantly correlated with abundances of bacteria than those of diatoms and cryptophytes (Kirchman et al. 2017). Metabarcoding analysis revealed that rainfall-induced nutrient loadings in Sydney Harbor, Australia, prompted shifts in microbial assemblages, with areas of greatest human impact exhibiting both harmful dinoflagellate (*Prorocentrum cordatum*) blooms and changes in bacterial (e.g. *Synechococcus*, SAR 11) abundances (Ajani et al. 2023). Since these and similar studies show that phytoplankton–bacterial associations are responsive to regional anthropogenic influences, characterizing their synergistic population dynamics within estuaries that are susceptible to chronic nutrient enrichment will markedly improve nutrient budgets and our overall understanding of urban ecosystem function.

One such system, Long Island Sound (LIS), located between the southern coast of Connecticut (CT), and Long Island, New York (NY), USA, is an estuary of national significance that supports numerous ecosystem services to its surrounding communities (Latimer et al. 2014). LIS receives N inputs from multiple sources, including rivers, atmospheric deposition, groundwater, remineralization, and wastewater, such as from combined sewage overflows (CSOs) and wastewater treatment plants (WTPs) (Latimer et al. 2014, Tamborski et al. 2017, Vlahos et al. 2020). Specifically, it receives N inputs from the greater New York City (NYC) metropolitan area such that 2.9×10^6 kg yr^{-1} of total trade-equalized N-loadings (the calculated N input values decline with increasing distance from NYC) were discharged to LIS from WTPs in 2022 alone (Long Island Sound Study 2023). The East River, where much of the CSO-sourced total N (TN) enters the estuary, connects NYC to the western LIS (WLIS) (Vlahos et al. 2020). Additionally, LIS receives ~90% of its freshwater from several rivers along its full northern shore (Van Patten et al. 2009). These features contribute to a general west (from NYC) to east (toward the Atlantic Ocean) trend of decreasing N (total and inorganic forms), bacterial abundances, as well as both total phytoplankton biomass (as chlorophyll *a*, [chl *a*]) and the relative contribution of picoplankton (<5 µm cell size) to total chl *a* (Suter et al. 2014, Vlahos et al. 2020, Humphries et al. 2023, Roldan-Ayala et al. 2023). By comparison, along the north shore of WLIS, concentrations of N, particularly ammonia (NH_3) + ammonium (NH_4^+), and chl *a* are positively and significantly correlated in areas nearby point-source wastewater inputs such that overall levels do not necessarily scale with distance from NYC (Brown et al. 2024). Given these contrasting spatial gradients, it is reasonable to surmise that WLIS regions near terrestrial or urban N sources (e.g. shore sites adjacent to wastewater outfalls and mid-channel sites closest to the East River–WLIS confluence) not only support the greatest phytoplankton biomass but also that the associated phytoplankton community is composed of taxa, such as

dinoflagellates (per Kirchman et al. 2017), with levels that correspond to bacterial population numbers.

Temporally, both WLIS phytoplankton biomass and bacterial populations reach a maximum during the summer coincident with increased temperatures and available N (Anderson & Taylor 2001, Liu et al. 2015, Roldan Ayala et al. 2023, Brown et al. 2024), though bacterial abundances have significantly correlated with chl *a* at 2.0 m depth (near sub-chlorophyll maximum) at only one WLIS mid-channel sampling site (Humphries et al. 2023). Presumably, numbers of the accompanying bacterial assemblage would increase with phytoplankton abundances, with this response more pronounced along the WLIS shore than the mid-channel, especially in areas closest to point source nutrient (such as N) inputs. Despite this assumption, variance in bacterial biomass has not been closely associated with chl *a* in WLIS surface waters (Anderson & Taylor 2001, Taylor et al. 2003). The disconnect between levels of phytoplankton biomass and bacterial abundances is complicated by the fundamental hydrographic differences between the WLIS mid-channel and shore, with the former driven by ocean–East River exchange and the latter being more influenced by terrestrial inputs (Gay et al. 2004, Long Island Sound Study 2015). However, in nearby LIS embayments (Shinnecock Bay and the Peconic Estuary), blooms of harmful dinoflagellate *Margalefidinium polykrikoides* were not only accompanied by significantly more heterotrophic bacteria, but microbial community composition was also altered during bloom versus non-bloom periods (Koch et al. 2014). Thus, connections between phytoplankton and bacteria may exist at a taxonomic (species) level in WLIS. Analyses into these potential associations have not been conducted on the CT shore, leaving a notable gap in reconciling how terrestrial inputs on the river-dominated shore may impact these populations.

Analyzing phytoplankton taxa and bacterial abundances as they relate to DOM can enhance the understanding of regional population dynamics, particularly how proximity to urban nutrient inputs (primarily wastewater) may increase microbial abundances, impact public health, and alter the food web and biogeochemical cycling. Specific phytoplankton taxa in LIS have been connected to DOM production, particularly Prasinophyceae and Cryptophyceae, which may release DON (Suter et al. 2014). Recent work has identified gradients in WLIS DOM amount and quality near outfalls, showing that colored DOM (CDOM) and chl *a* were correlated, indicating increased autochthonous CDOM production in response to wastewater inputs (Menendez & Tzortziou 2024). WLIS DOC concentrations are typically highest during summer (Vlahos & Whitney 2017), when primary productivity is at its peak. Information on how specific phytoplankton taxa influence DOM concentrations is lacking in WLIS. However, in other estuaries, phytoplankton can contribute substantially to DOM, as autochthonous DOC can make up the bulk estuarine DOC pool (for example, in the Camden Haven estuary, Australia; Maher & Eyre 2011) and peak when phytoplankton biomass and productivity are highest (Keller & Hood 2011). Thus, autochthonous DOM components (DON, DOP, and DOC) may be indirectly altered by proximity to point-source nutrient sources in WLIS as a consequence of the present phytoplankton community.

The goal of this project was to identify and compare associations between key phytoplankton taxa and bacterial abundances in WLIS (2020–2021), as they relate to DOM at mid-channel and shore locations. This study tested the hypotheses that (1) the WLIS shore will have higher overall phytoplankton biomass and abundances of both phytoplankton and bacteria than the mid-channel, with shore sites in closest proximity to wastewater inputs exhibiting the highest levels of DOM and microbial abundances, and that (2) dinoflagellates will be more abundant in areas closest to wastewater sources, corresponding to higher bacterial populations. Specific objectives were to (1) quantify bacterial abundances in waters across an urban–suburban gradient in 2 WLIS regions: the mid-channel and along the north (NY–CT) shore; and (2) assess bacterial associations with phytoplankton (biomass, abundances of major taxa), DOM levels, and physical water quality within and among both regions and seasons. Resultant data will help elucidate linkages between specific DOM components with phytoplankton and bacteria as well as improve our understanding of microbial population dynamics and biogeochemical cycling within WLIS and other urban estuaries worldwide.

2. MATERIALS AND METHODS

2.1. Sample collection and physical water quality

Water was collected monthly (20 July 2020 to 5 October 2021), with July and August sampled 2 and 3 times, respectively, during ebb tide from the WLIS mid-channel, and monthly (20 November 2020 to 4 October 2021) along the shore. Mid-channel collections leveraged long-term hypoxia and water-quality monitoring surveys conducted by the Connecticut

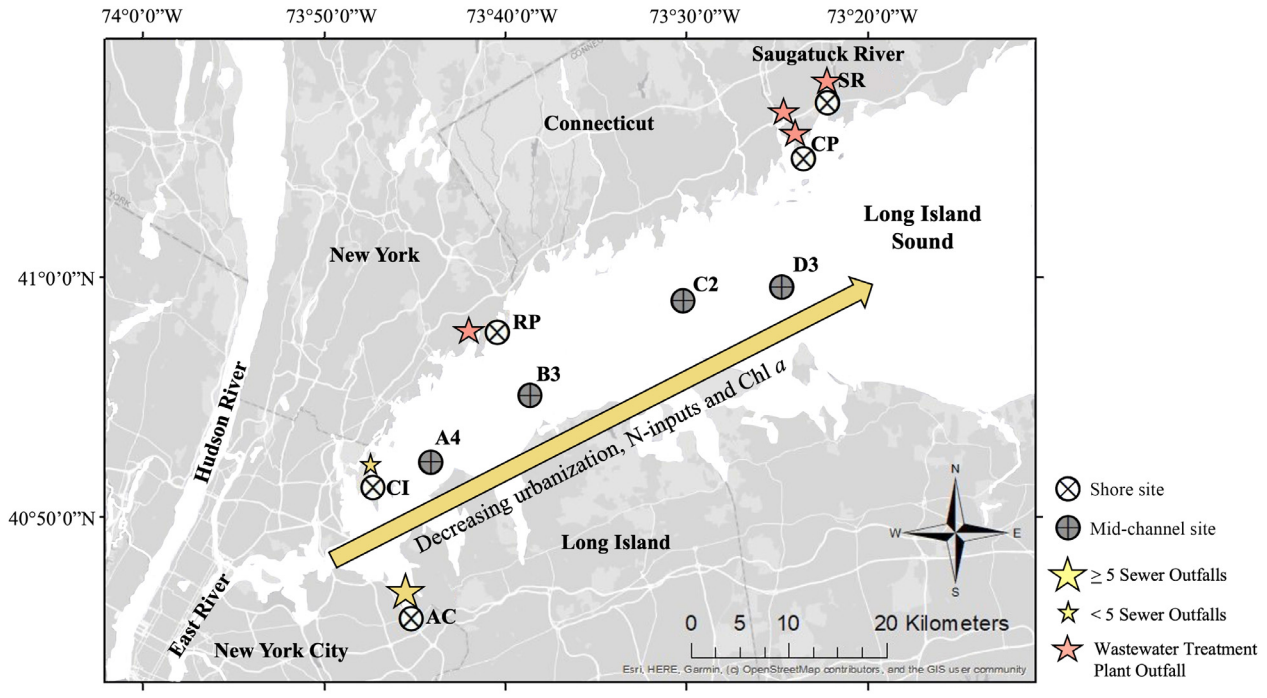

Fig. 1. Study region (Western Long Island Sound, USA) showing sampling sites relative to an urban–suburban gradient of increasing nitrogen and chl *a* concentrations (yellow arrow) toward New York City. Mid-channel sites (Sites A4, B3, C2, and D3) and shore sites (Sites AC [Alley Creek], CI [City Island], RP [Rye Playland], CP [Calf Pasture] and SR [Saugatuck River]) are shown

Department of Energy and Environmental Protection (CTDEEP) at Sites A4, B3, C2, and D3 (Fig. 1) spanning an urban (NYC)–suburban (CT) (west-to-east) gradient, with Site A4 closest to NYC and the East River (CTDEEP 2021, Roldan-Ayala et al. 2023). Shore sites included Alley Creek (AC), City Island (CI), Rye Playland (RP), Calf Pasture (CP), and Saugatuck River (SR) (Fig. 1), covering the primary NYC–CT commuting corridor (Brown et al. 2024). Site SR was located ~620 m (0.39 mi) downstream from the nearest WTP outfall while Site CP was ~2472 m (1.54 mi) downstream from the nearest outfall. Site RP was ~1763 m (1.10 mi) away from a WTP, though physically and hydrographically separated by a landmass (Rye Town). Of all sites, AC was in closest proximity to 5 CSO outfalls (~425 m [0.26 mi] distance), and CI was ~1048 m [0.65 mi]) away from 2 CSO outfalls.

Mid-channel physical water quality (temperature [*T*], salinity [S]) was measured using a CTD (conductivity, temperature, and depth; Sea-Bird model SBE-19 SeaCat Profile). Dissolved oxygen (DO) and pH were measured using a YSI EXO2 data sonde. At each site, water samples (n = 3) were collected from surface depth (0.5 m) via a rosette sampler equipped with 5 l Niskin bottles. Water was then dispensed into 1 l Nalgene© amber wide-mouth bottles, previously soaked in 10% hydrochloric acid (HCl) for a minimum of 24 h then rinsed 3 times with reverse osmosis water and 3 times with analytical grade deionized (DI) water (PURELAB® Chorus Water Purification System; water purity of 18.2 MΩ cm^{-1}). At each shore site, water quality (*T*, S, DO, pH, and turbidity) was measured using a YSI EXO2 data sonde, then samples were collected from surface depth using a 2 l Niskin bottle and dispensed into 1 l Nalgene© bottles (treated as above), in triplicate. All water samples were transported in a cooler with icepacks to the City University of New York (CUNY) Advanced Science Research Center within 2 h of shore arrival (mid-channel) or collection (shore). Each replicate was then gently rotated 10 times to ensure the water was well-mixed, then processed for phytoplankton biomass (using chl *a* as a proxy) and community composition, nutrients, and bacteria as follows.

2.2. Chl *a*

For each replicate, aliquots (40 ml) of water were condensed onto 25 mm, 0.7 µm pore size glass microfiber filters (GF/Fs) (Whatman®) using a vacuum pump (5 mm Hg) to measure total chl *a*. Two additional 40 ml aliquots were subsequently passed through 20 and 5 µm Nitex® nylon meshes and con-

densed onto GF/Fs as above to assess the relative contributions of micro- (>20 µm), nano- (5—20 µm), and picoplankton (<5 µm) cell diameter size fractions to total chl *a*. Filters were placed into 20 ml plastic scintillation vials and frozen (−20°C) until pigment extraction (−20°C for 36—48 h), which occurred within 0—2.5 wk of freezing to prevent substantial chl *a* loss (Graff & Rynearson 2011) (see Table S2). Concentrations were measured by thawing the extracted samples in the dark and evaluating them using pre-sonicated 5 ml borosilicate glass test tubes and a Turner Designs© Trilogy Laboratory Fluorometer, non-acidification module (Welschmeyer 1994, Turner Designs 2017). Mean chl *a* values for mid-channel (Roldan-Ayala et al. 2023) and shore (Brown et al. 2024) sites are used here.

2.3. Phytoplankton community composition

To determine phytoplankton community composition, ~18 ml from each replicate was fixed with 200 µg l^{-1} Lugol's iodine solution in 20 ml amber glass vials and stored in the dark at 4°C until analysis. Samples were evaluated by dispensing 1 ml of stained sample into a gridded Sedgewick rafter counting chamber and then viewing with an Olympus (BX53) compound light microscope (10× objective). Phytoplankton community composition was determined by identifying cells to the lowest taxonomic level possible then counting at least 300 cells per species or the whole chamber if the minimum threshold was not reached. Most species <5 µm were too small to be accurately identified and therefore excluded from counts. Mean (n = 3) cell concentrations per phytoplankton species were calculated (LeGresley & McDermott 2010, Roldan-Ayala et al. 2023, Brown et al. 2024), pooled according to major taxa (centric diatoms, pennate diatoms, dinoflagellates, euglenoids, raphidophytes, cryptophytes), and then summed per sampling date and site. Rare taxa (<5% of overall cell abundances) were omitted from the analysis.

2.4. Bacterial abundances

Aliquots (18 ml) of water from each replicate were filtered through a 20 µm Nitex® nylon mesh into amber glass vials containing 20% phosphate-buffered saline (PBS)-buffered formaldehyde and stored at 4°C (for the PBS-buffered formaldehyde formula, see Humphries et al. 2023). Thermo Fisher Scientific™ 4′,6-diamidino-2-phenylindole (DAPI) stock solution and working solution were prepared according to Thermo Fisher Scientific™ specifications (Porter & Feig 1980, Thermo Scientific 2010) and stored frozen (−20°C) for ~1 mo. Sample filters were stained using 30 ml glass towers clamped onto a manifold with 25 mm, 1.6 µm pore size, GF/A grade backing filters, and DI-washed Isopore™ 0.2 µm black polycarbonate membrane filters. Each tower received 2 ml of sample and 20 µg of DAPI working stock and underwent a 5 min darkened incubation with a subsequent 3 ml PBS-buffered formalin rinse (3 times).

Stained filters were mounted onto glass slides with Corning© 25 mm glass coverslips and stored (−20°C) in the dark until imaging and quantification using a Nikon ECLIPSE Ni upright epifluorescent microscope at 40×/0.80 W (400× magnification) equipped with NIS-Elements AR 5.21.03 software (Nikon 2015). Samples were viewed via 40× DAPI and Sola light to display the image of 460 × 460 µm (211 600 $µm^2$) viewfield then imaged 15× (at random). The 'object count' function and parameter specifications used to quantify bacterial cell numbers are detailed in Humphries et al. (2023).

2.5. DOM

To determine DOM concentrations, water samples (~18 ml) were filtered with a 30 ml syringe through a GF/F into acid-washed (as described in Section 2.1) 20 ml glass scintillation vials for total dissolved N (TDN) and phosphorus (TDP). Sample vials were then frozen (−20°C) until analysis using a Hach© Lachat QuikChem 8500 Flow Injection Analysis System (Strickland & Parsons 1984, Grasshoff et al. 1999). The lower limits of detection (LLD) for TDN and TDP were 0.485 and 0.123 µM, respectively (Tucker et al. 2008a,b). When resultant data were below the LLD, concentrations were set to the corresponding LLD value. DON and DOP concentrations were calculated per replicate as TDN — dissolved inorganic N (DIN) and TDP — dissolved inorganic phosphorus (DIP), respectively, using DIN and DIP values from Roldan-Ayala et al. (2023) (mid-channel) and Brown et al. (2024) (shore) sites. DOC samples were collected by filtering water through pre-combusted GF/F filters into 20 ml glass scintillation vials (Ducklow & Dickson 1994, JGOFS 1996). Following acidification with 10% HCl, the vials were stored (4°C) prior to analysis in duplicates by the University of Wisconsin—Milwaukee. DOM was calculated as the sum of DON, DOP, and DOC.

2.6. Statistical analyses

Using R Studio (version 2022.12.0 + 353), data for all metrics were tested for normality (Shapiro-Wilk). All data sets for chl *a*, DON, DOP, and DOC concentrations, phytoplankton abundances, and water quality metrics were $\ln(x + 1)$ transformed. Bacterial abundances were $\log_{10}$ transformed. All transformed data sets were then re-tested for normality, and only euglenoid abundance data remained non-normally distributed. Pearson correlations were used to test associations among the major phytoplankton taxa, chl *a* (total and individual cell size fractions), bacterial abundances, DON, DOP, DOC, and physical water quality (*T*, S, DO, pH, and turbidity). In addition, the most abundant phytoplankton genera (the dinoflagellates *Prorocentrum* spp. and *Heterocapsa* as well as the centric diatoms *Leptocylindrus* spp., *Skeletonema*, and *Thalassiosira* spp.) were compared to bacterial abundances, DON, DOP, and DOC. All associations between parameters (bacterial abundances, DON, DOP, DOC, and physical water quality) and euglenoid cell abundances were tested using non-parametric Spearman rank correlations. See Table S1 for Pearson and Spearman rank correlation p and r values.

Two sample *t*-tests assuming equal variance were used to compare the pooled means of all shore versus all mid-channel sites for phytoplankton taxa, bacterial abundances, and concentrations of total chl *a*, DON, DOP, and DOC for 3 seasons (defined by solstices and equinoxes) as fall, spring, and summer; winter was excluded due to lack of statistical power. Specifically, these *t*-tests were used to compare the pooled means of phytoplankton and bacterial abundances as well as chl *a* concentrations between the 2 site regions. Significance for all tests was defined as a 95% confidence interval ($p < 0.05$).

A principal component analysis (PCA) was used to evaluate relationships between all metrics pooled for each site type, excluding physical water quality. The PCA was conducted on data normalized to have zero mean and unit variance using the 'FactoMineR' package. The first 2 principal components (Dim1 and Dim2) were visualized using the 'fviz_pca_biplot' function from the 'Factoextra' package. This visualization included a representation of the cosine squared (cos2) values for each variable on these dimensions, which ranged from 0.00 to 0.25, indicating the proportion of variance each variable contributes to the principal components.

3. RESULTS

3.1. Physical water quality

Mean (±SE) *T* (13.47 ± 1.88°C) of the WLIS mid-channel was generally warmer than the shore (11.67 ± 1.64°C) across all sites and seasons (Tables 1 & 2), with little variation between individual sites per region. *T*

Table 1. Means (n = sampling dates per season) and ranges (in parentheses, where n > 1) for water temperature (*T*), salinity (S), dissolved oxygen (DO), and pH measurements for mid-channel sites (see Fig. 1) during 2020 and 2021 combined

Season	*T* (°C)	S	DO (mg l^{-1})	pH
Site A4				
Fall (n = 2)	17.48 (13.70–20.85)	26.55 (25.73–27.30)	8.28 (7.64–9.43)	8.18 (7.83–8.80)
Winter (n = 1)	3.30	26.59	13.15	8.11
Spring (n = 3)	12.90 (8.20–17.60)	26.09 (26.04–26.13)	10.33 (9.34–11.32)	9.82 (9.25–10.38)
Summer (n = 8)	23.50 (22.07–25.00)	26.02 (25.07–26.69)	7.74 (6.66–9.24)	7.94 (7.55–8.31)
Site B3				
Fall (n = 2)	18.96 (13.50–25.28)	27.11 (26.09–27.97)	8.51 (8.05–9.12)	8.13 (7.94–8.45)
Winter (n = 1)	3.10	26.91	12.99	8.16
Spring (n = 3)	14.40 (10.40–18.40)	26.13 (26.01–26.25)	10.40 (8.94–11.86)	9.39 (9.29–9.48)
Summer (n = 8)	23.01 (18.40–25.40)	26.33 (25.34–26.96)	8.14 (7.59–9.05)	8.22 (7.88–9.29)
Site C2				
Fall (n = 2)	21.44 (18.60–24.27)	27.63 (26.83–28.43)	7.80 (7.75 0 7.84)	7.90 (7.86–7.94)
Winter (n = 1)	2.60	27.53	12.32	8.02
Spring (n = 3)	12.30 (6.50–18.10)	27.01 (26.47–27.54)	9.18 (8.77–9.59)	10.49 (8.97–12.01)
Summer (n = 8)	22.49 (18.10–24.40)	26.62 (25.65–27.58)	7.95 (6.98–9.59)	9.09 (7.80–8.97)
Site D3				
Fall (n = 2)	19.34 (14.40–24.81)	28.01 (26.88–28.89)	9.73 (8.86–10.84)	8.07 (7.92–8.29)
Winter (n = 1)	3.10	27.47	11.83	8.18
Spring (n = 3)	14.05 (8.50–19.60)	27.02 (26.97–27.06)	9.78 (8.99–10.57)	10.55 (10.52–10.57)
Summer (n = 8)	23.60 (19.60–26.40)	26.69 (25.56–27.63)	7.97 (7.09–9.03)	8.36 (7.90–10.52)

Table 2. Means (n = 3 sampling dates per season) and ranges (in parentheses) for water temperature (*T*), salinity (S), dissolved oxygen (DO), pH, and turbidity measurements for shore sites (see Fig. 1) during 2020 and 2021 combined

Season	*T* (°C)	S	DO (mg l^{-1})	pH	Turbidity (FNU)
Site AC					
Fall	12.41 (5.30–20.84)	26.42 (25.45–27.70)	7.70 (5.43–9.32)	7.67 (7.59–7.75)	6.21 (4.87–7.54)
Winter	1.07 (0.01–2.00)	15.65 (11.00–21.10)	11.10 (10.32–11.59)	7.57 (7.44–7.70)	45.50 (39.43–57.10)
Spring	10.55 (8.20–12.90)	21.06 (21.06–22.30)	7.08 (6.29–7.86)	7.34 (7.27–7.40)	6.06 (5.30–6.82)
Summer	21.26 (18.78–23.70)	17.94 (6.18–25.14)	5.42 (2.46–10.75)	7.28 (6.96–7.86)	23.40 (5.30–45.88)
Site CI					
Fall	13.62 (7.90–21.25)	28.88 (27.44–29.80)	8.46 (6.83–9.39)	7.82 (7.70–7.98)	2.37 (0.70–5.29)
Winter	2.20 (0.60–4.10)	28.24 (27.82–28.60)	11.99 (11.71–12.29)	8.13 (8.05–8.29)	2.28 (0.90–4.30)
Spring	9.15 (6.90–11.40)	28.33 (28.25–28.41)	9.88 (9.12–10.64)	7.96 (7.88–8.04)	0.67 (0.63–0.71)
Summer	22.09 (21.60–22.67)	27.58 (26.66–28.24)	6.67 (5.55–8.44)	7.66 (7.50–7.90)	1.79 (0.56–3.16)
Site CP					
Fall	11.82 (7.20–20.36)	26.34 (21.80–29.10)	9.03 (7.35–10.18)	7.88 (7.79–8.02)	3.27 (1.17–4.54)
Winter	2.70 (1.40–4.60)	28.60 (28.41–28.90)	11.46 (11.06–11.70)	8.13 (8.05–8.27)	3.07 (1.36–4.11)
Spring	9.55 (6.70–12.40)	27.90 (27.54–28.25)	10.26 (9.24–11.28)	8.04 (7.94–8.14)	1.09 (0.80–1.38)
Summer	22.38 (22.20–22.65)	27.75 (26.85–28.80)	6.88 (6.64–7.15)	7.72 (7.69–7.78)	3.31 (2.03–5.44)
Site RP					
Fall	13.20 (8.10–21.20)	29.78 (28.54–30.50)	8.29 (6.59–9.29)	7.85 (7.77–7.94)	1.06 (0.70–1.49)
Winter	2.53 (1.10–4.40)	28.84 (28.41–29.10)	11.66 (11.25–12.02)	8.17 (8.07–8.24)	2.76 (0.79–4.00)
Spring	8.60 (6.10–11.10)	28.94 (28.78–29.10)	9.55 (8.87–10.22)	7.94 (7.88–8.00)	0.93 (0.90–0.95)
Summer	22.02 (21.30–22.66)	28.27 (27.64–28.74)	7.07 (5.54–8.82)	7.78 (7.53–8.05)	1.71 (1.15–2.41)
Site SR					
Fall	11.48 (6.40–20.15)	20.80 (18.00–22.60)	8.82 (6.48–10.44)	7.71 (7.53–7.80)	2.64 (0.87–4.83)
Winter	2.93 (1.80–3.90)	18.77 (14.49–21.57)	12.13 (11.28–12.88)	8.06 (7.90–8.24)	4.28 (1.24–8.90)
Spring	11.00 (8.10–13.90)	14.78 (14.13–15.43)	10.76 (9.55–11.97)	8.00 (7.86–8.13)	1.36 (1.08–1.64)
Summer	22.92 (21.17–24.00)	14.80 (3.78–23.94)	7.81 (7.37–8.43)	7.56 (7.18–7.77)	7.72 (3.84–14.79)

was negatively correlated with abundances of both pennate diatoms for mid-channel sites pooled (Pearson's r = −0.680, p = 0.008) and centric diatoms for shore sites pooled (r = −0.690, p = 0.030), but it was positively correlated with dinoflagellate abundances at both mid-channel (r = 0.690, p = 0.006) and shore sites pooled (r = 0.640, p = 0.033; Table S1 in the Supplement at www.int-res.com/articles/suppl/a090p121_supp.pdf).

The WLIS mid-channel was generally more saline than the shore, with a mean S of 25.61 ± 1.29 compared to 24.48 ± 1.21, respectively (Tables 1 & 2), with Sites AC and SR having the lowest mean S. Pooled mid-channel S was negatively correlated with both dinoflagellate abundances (r = −0.550, p = 0.041) and total chl *a* concentrations (r = −0.570, p = 0.035; Table S1). No significant correlations were found between S and other metrics at the shore. Mean DO levels were slightly higher for mid-channel sites pooled (9.76 ± 0.48 mg l^{-1}) than along the shore pooled (9.10 ± 0.45 mg l^{-1}) (Tables 1 & 2), with hypoxia occurring at Site AC, the site nearby 5 CSO outfalls, on 3 September 2021 (DO: 2.46 mg l^{-1}; Table 2). DO levels were negatively and significantly correlated with bacterial abundances at both individual shore sites and shore sites pooled (r = −0.920, p < 0.001; Table S1), indicating respiration. Overall, the mean pH (7.82 ± 0.06) was lower along the shore than the mid-channel (8.66 ± 0.23) (Tables 1 & 2). While there were no clear correlations between turbidity and other parameters across shore sites (Table S1), Site AC was more turbid during summer than any other site or season (mean: 23.40 ± 6.01 FNU; Table 2).

3.2. Chl *a*

Across seasons, total chl *a* concentrations were generally, but not significantly, lower in the mid-channel than along the shore. Mid-channel chl *a* concentrations averaged across sites ranged from 1.96 to 14.08 µg l^{-1}, with a mean of 8.41 ± 1.16 µg l^{-1}. Mean chl *a* concentrations were greatest July through August during both years (Table S2), such that values were highest at the most western (closest to NYC) station, Site A4 (12.81 ± 2.32 µg l^{-1}), and lowest at the most eastern site, Site D3 (4.86 ± 0.72 µg l^{-1}). These data coincided with higher phytoplankton cell counts, primarily euglenoids and dinoflagellates, closest to

NYC. For mid-channel sites pooled, chl *a* concentrations for both total and the <5 µm cell size fraction were positively correlated with bacterial abundances (Pearson's r = 0.630, p = 0.015; r = 0.610, p = 0.020, respectively), though individual mid-channel sites showed no significant correlations between chl *a* and bacteria (Table S1).

Along the shore, total chl *a* concentrations for sites pooled ranged from 1.34 to 53.37 µg l^{-1}, with a mean of 11.72 ± 4.34 µg l^{-1} (Table S2). Mean chl *a* levels were elevated in July–August and October 2021 (Table S2), highest at Site AC (28.20 ± 15.76 µg l^{-1}), and lowest at Site CP (4.56 ± 0.80 µg l^{-1}). Elevated chl *a* levels coincided with higher cell abundances of euglenoids and dinoflagellates across all stations, with this trend most prominent at Site AC. Similar to the mid-channel, total and <5 µm chl *a* concentrations were positively correlated with bacterial abundances for shore sites pooled (r = 0.690, p = 0.013; r = 0.830, p = 0.001, respectively). Chl *a* concentrations (>20 µm cell size fraction) were only positively correlated with bacterial abundances at Site SR (r = 0.580, p = 0.046), while the 5–20 µm size fraction positively correlated with bacteria at both Site CI (r = 0.710, p = 0.010) and Site SR (r = 0.600, p = 0.040). The <5 µm cell size fraction positively correlated with bacterial abundances across all sites except RP, the only one lacking a defined terrestrial input source, as Sites AC (r = 0.600, p = 0.039), CI (r = 0.810, p = 0.001), CP (r = 0.730, p = 0.007), and SR (r = 0.660, p = 0.020; Table S1). Total chl *a* concentrations were not significantly different between the mid-channel and shore during any season (Table S3).

3.3. Phytoplankton community composition

Across the study, mid-channel dinoflagellate and bacterial abundances were positively correlated at Site A4 (Pearson's r = 0.520, p = 0.048), Site C2 (r = 0.570, p = 0.037), and all sites pooled (r = 0.650, p = 0.013; Table S1, Figs. 2 & 3). Euglenoid and bacterial abundances were also positively correlated for all sites pooled (Spearman's r = 0.547, p = 0.043), whereas cryptophytes negatively correlated with bacterial abundances at Site A4 (Pearson's r = −0.560, p = 0.030; Table S1). The most abundant diatom genera in the mid-channel were *Leptocylindrus*, *Skeletonema*, and *Thalassiosira*, while the most abundant dinoflagellate genera were *Scrippsiella* and *Prorocentrum*; bacterial abundances were positively correlated with those of *Prorocentrum* spp. for all sites pooled (r = 0.610, p = 0.015; Table S4).

Compared to the mid-channel, the positive correlation between dinoflagellate and bacterial abundances was stronger at shore sites CI (r = 0.880, p < 0.001), CP (r = 0.750, p = 0.005), and all sites pooled (r = 0.750, p = 0.005; Table S1, Figs. 2 & 3). Euglenoid and bacterial abundances were positively correlated at Site AC (r = 0.831, p = 0.001) and all sites pooled (r = 0.671, p = 0.020; Table S1). The most abundant shore diatom genera were *Skeletonema* and *Thalassiosira*, while the most abundant dinoflagellate genera were *Heterocapsa* and *Prorocentrum.* As with the mid-channel, bacterial abundances positively correlated with dinoflagellates at sites pooled, and this effect was highly significant for *Prorocentrum* spp. (r = 0.880, p <0.001) as well as significant for *Heterocapsa* (r = 0.610, p = 0.035; Table S4).

Pooled phytoplankton taxa abundances were overall greater at the shore than at mid-channel sites, but the statistical significance of this effect depended upon the taxon and season (Fig. 4, Table S3). This was primarily attributed to relatively higher summer abundances of centric diatoms (two-sample *t*-test, *t* = 5.304, p = 0.006, df = 11), pennate diatoms (*t* = 4.859, p = 0.008), cryptophytes (*t* = 7.480, p = 0.002), and raphidophytes (*t* = 1.323, p = 0.046), coincident with significantly higher summer bacterial abundances (detailed in Section 3.4). Shore sites also had relatively more cryptophytes (*t* = 22.432, p < 0.001) and raphidophytes (*t* = 2.547, p = 0.004) during spring. Neither dinoflagellate nor euglenoid abundances were significantly different between mid-channel and shore sites pooled over any season (Table S3).

3.4. Bacterial abundances

Mid-channel bacterial abundances ranged from 5.92 × 10^3 to 3.27 × 10^5 cells ml^{-1} (Fig. 5) and were highest in July during both years. Peak abundances (3.27 × 10^5 cells ml^{-1}) were recorded at Site A4, the site closest to NYC, during July 2021. Bacterial abundances were negatively and significantly correlated with DON concentrations at all mid-channel sites pooled (Pearson's r = −0.570, p = 0.033) but otherwise not significantly correlated with DON. Shore bacterial abundances ranged from 1.07 × 10^4 to 3.68 × 10^5 cells ml^{-1} and were typically greater than the mid-channel; this difference was significant during summers pooled (two-sample *t*-test, r = 2.867, p = 0.046; Table S3). The highest abundances (3.68 × 10^5 cells ml^{-1}) occurred during August at Site AC (peak abundances for Site SR occurred in September and for Site CP in October, both years). Bacterial abundances were positively cor-

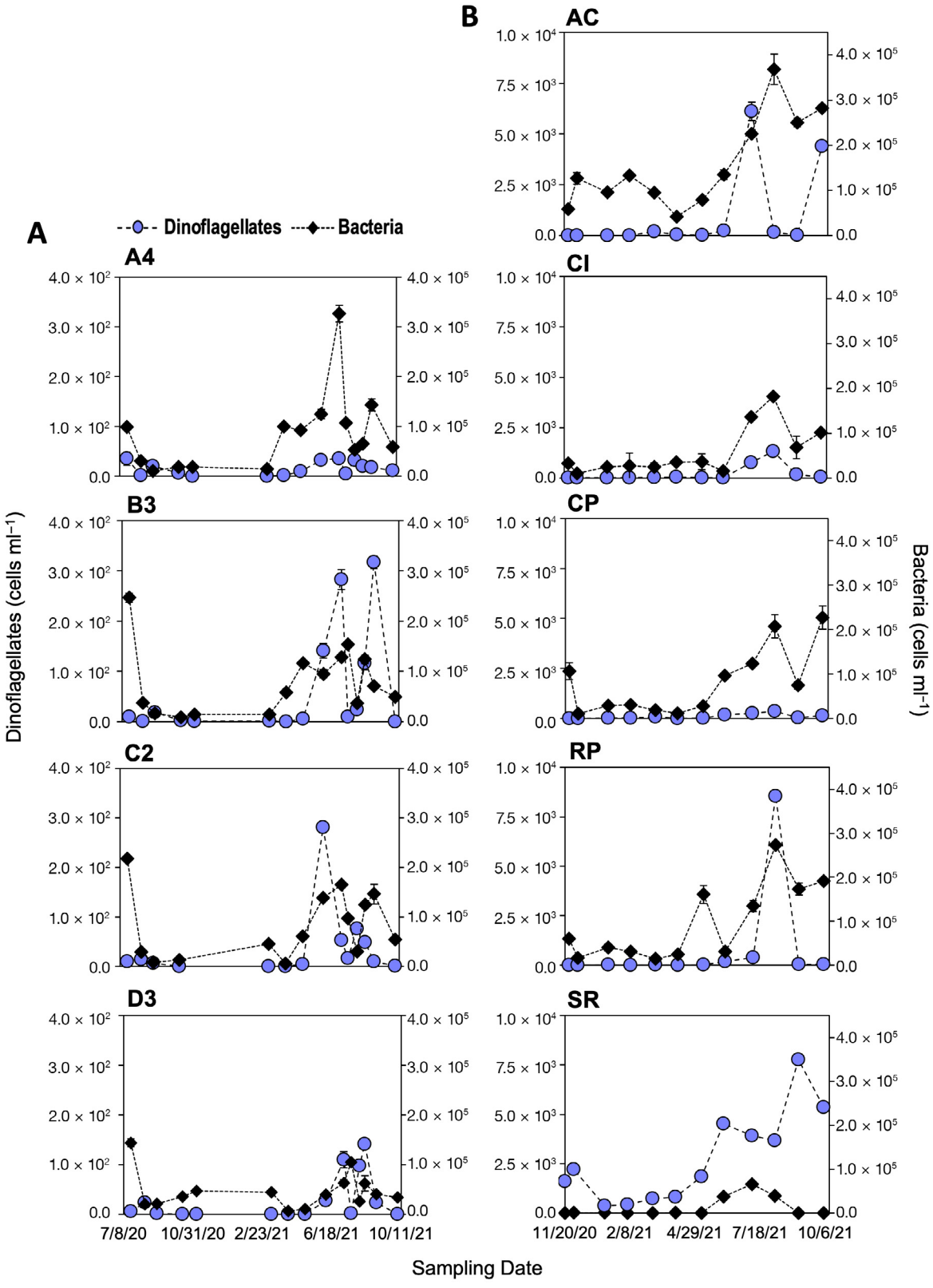

Fig. 2. Mean (±SE) dinoflagellate and bacteria cell abundances summed per sampling date (given as mo/d/yr) for each (A) mid-channel and (B) shore site (labelled at the top-left corner of each panel; see Fig. 1 for explanation of site abbreviations). Markers cover error bars for many dinoflagellate mean abundances. Note the difference in *y*-axis scales for dinoflagellates and bacteria

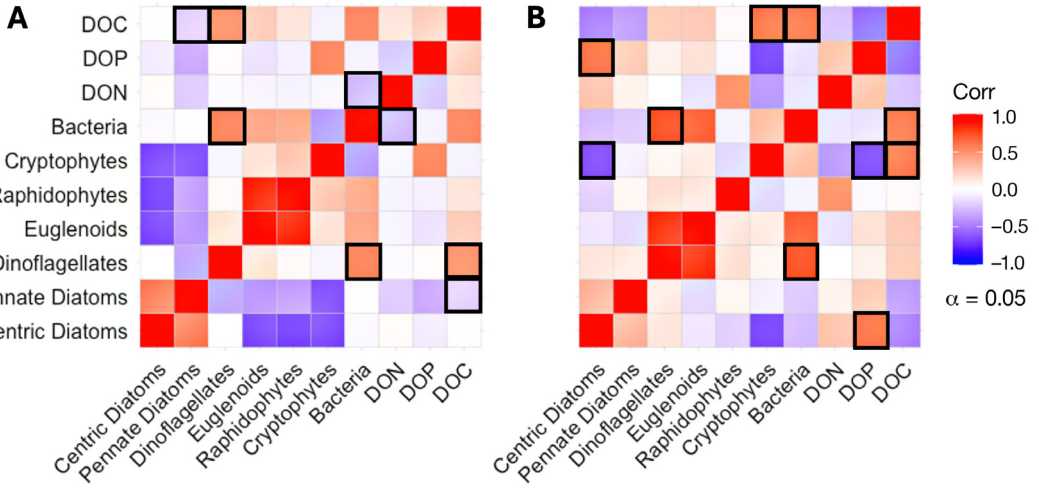

Fig. 3. Pearson correlation heat maps for abundances of major phytoplankton taxa, bacterial abundances, and concentrations of dissolved organic nitrogen, phosphorus and carbon (DON, DOP, and DOC) at (A) mid-channel and (B) shore sites (see Fig. 1) pooled (2020 and 2021). Red: strength of positive correlations; blue: strength of negative correlations between metrics on the *x*- and *y*-axes. Black boxes indicate statistically significant correlations between metrics. The corresponding p- and r-values are provided in Table S1

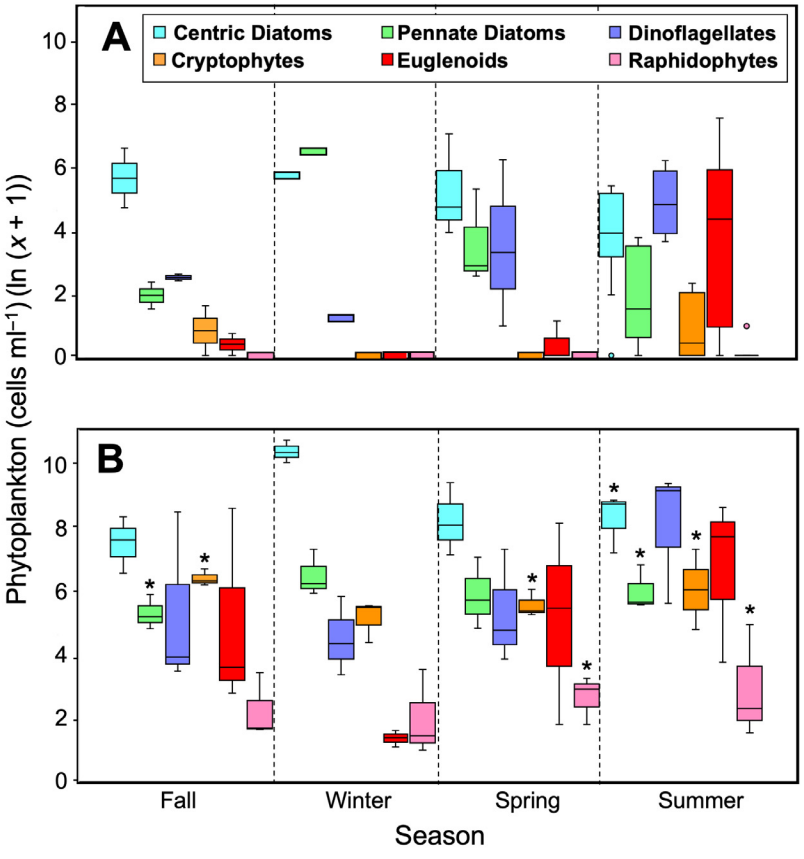

Fig. 4. ln(*x* + 1)-transformed phytoplankton taxa abundances from (A) mid-channel and (B) shore sites depicting medians and quartiles (whiskers) throughout each season (delineated by dashed lines) for 2020 and 2021 combined. Orange dot depicts a single outlier in summer mid-channel cryptophyte abundances. Asterisks (*) indicate cases where cell abundances at shore sites were significantly (α = 0.05) higher than mid-channel abundances (two-sample *t*-tests assuming equal variance). Winter *t*-tests are missing due to insufficient sampling dates

related with DOC concentrations at Site AC (r = 0.840, p = 0.001) and with all shore sites pooled (r = 0.640, p = 0.024; Table S1).

3.5. DOM

Concentrations of DOM were highest during the summer and fall for both regions, with DOC being the largest component of the DOM pool. DOC concentrations were significantly higher at shore than mid-channel sites across all tested seasons — fall (*t*-test, $t = 10.697$, $p < 0.001$), spring ($t = 3.874$, $p = 0.018$), and summer ($t = 7.661$, $p = 0.002$) — indicative of terrestrial DOM inputs. Shore DON concentrations were also significantly higher than the mid-channel during spring ($t = 7.609$, $p = 0.002$; Table S3).

Within the WLIS mid-channel, DOC concentrations ranged from 116.56 to 191.49 µM with a mean of 157.80 ± 2.76 µM (Fig. S1). DOC concentrations were negatively correlated with pennate diatom abundances at Sites B3 (Pearson's r = −0.660, p = 0.013), C2 (r = −0.770, p = 0.015), D3 (r = −0.680, p = 0.020), all mid-channel sites pooled (r = −0.730, p = 0.016), as well as with centric diatom abundances at B3 (r =

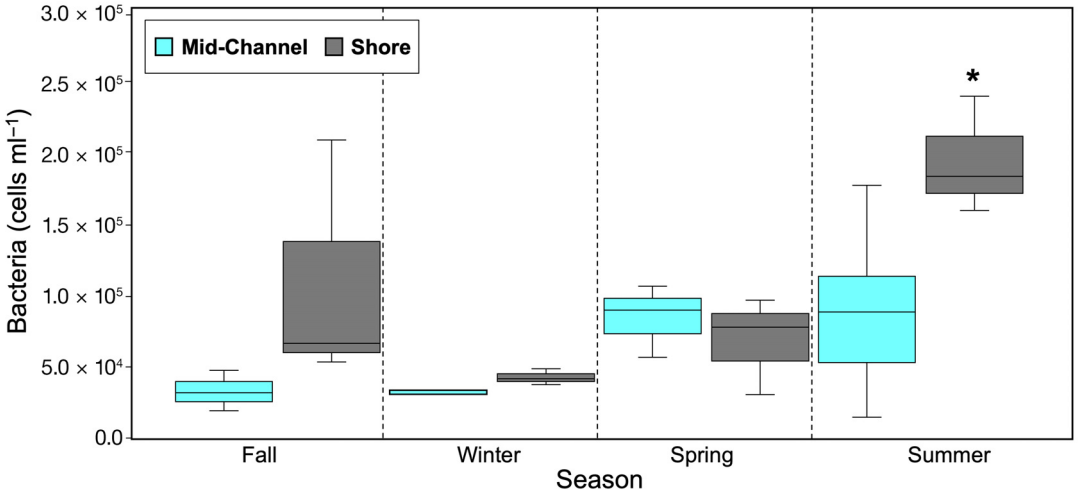

Fig. 5. Median bacterial abundances from mid-channel and shore sites depicting medians and quartiles (whiskers) throughout each season (defined by solstices and equinoxes) for 2020 and 2021 combined. Asterisk (*) indicates cases where cell abundances at shore sites were significantly ($\alpha = 0.05$) higher than mid-channel abundances (two-sample *t*-tests assuming equal variance). Winter *t*-tests are missing due to insufficient sampling dates

−0.720, p = 0.013; Table S1, Fig. 6). Conversely, DOC concentrations positively correlated with dinoflagellate abundances at all mid-channel sites pooled (r = 0.700, p = 0.024) (Table S1). Unlike DOC, mean mid-channel DON (65.66 ± 25.19 µM) and DOP (4.68 ± 2.28 µM) concentrations were generally, but not significantly, higher than at the shore (Fig. S1). DOC and DON levels pooled within mid-channel sites varied in tandem with population levels of common phytoplankton genera such that DOC positively correlated with *Prorocentrum* abundances (r = 0.740, p = 0.015) whereas DON concentrations negatively correlated with *Leptocylindrus* spp. abundances (r = −0.025, p = 0.046; Table S4).

At shore sites, DOC concentrations were higher than the mid-channel and ranged from 163.08 to 791.77 µM, with the mean of 344.28 ± 20.44 µM being higher than that of the mid-channel (Fig. S1). DOC concentrations were significantly and negatively correlated with abundances of pennate diatoms only at Site CP (r = −0.630, p = 0.040) and with centric diatoms at both Sites CP (r = −0.610, p = 0.019) and SR (r = −0.620, p = 0.033). By comparison, at AC (the CSO site), DOC concentrations were positively correlated with abundances of dinoflagellates (r = 0.600, p = 0.041), bacteria (r = 0.840, p = 0.001), and concentrations of total chl *a* (r = 0.680, p = 0.015). Mean shore DON and DOP concentrations were 43.34 ± 5.27 and 0.89 ± 0.21 µM, respectively (Fig. S1). Like the mid-channel, DOC concentrations were positively correlated with *Prorocentrum* abundances (Pearson's r = 0.660, p = 0.020) but negatively correlated with *Skeletonema* abundances (r = −0.720, p = 0.009; Table S4).

3.6. PCA analysis

PCA analyses (Fig. 7) demonstrated that the first 2 dimensions (Dim1 and Dim2) accounted for 76.8% of the variance in the data collected from the mid-channel and 83% of the variance observed at the shore. Notably, abundances of dinoflagellates, bacteria, and euglenoids were closely associated at both shore and mid-channel sampling locations. Conversely, DON exhibited an inverse relationship with dinoflagellates and bacteria across both regions.

4. DISCUSSION

4.1. Major findings

This study revealed that bacterial abundances are overwhelmingly associated with dinoflagellates, indiscriminate of region (mid-channel vs. shore), in the urban WLIS (Fig. 2). Findings imply that environmental conditions conducive to dinoflagellate population growth likely also enhance bacterial production and/or that bacteria augment WLIS dinoflagellate populations, similar to the developed Delaware Estuary (Kirchman et al. 2017). Conversely, the lack of observed linkages between diatom and bacterial abundances could be attributed to the negative association between pennate diatoms and DOC concentrations (Table S1), as pennate diatoms may either uptake DOC (Nilsson & Sundback 1996, Tuchman et al. 2006, Znachor & Nedoma 2010) or release it during cell death and lysis (Suttle 2005), thereby increasing

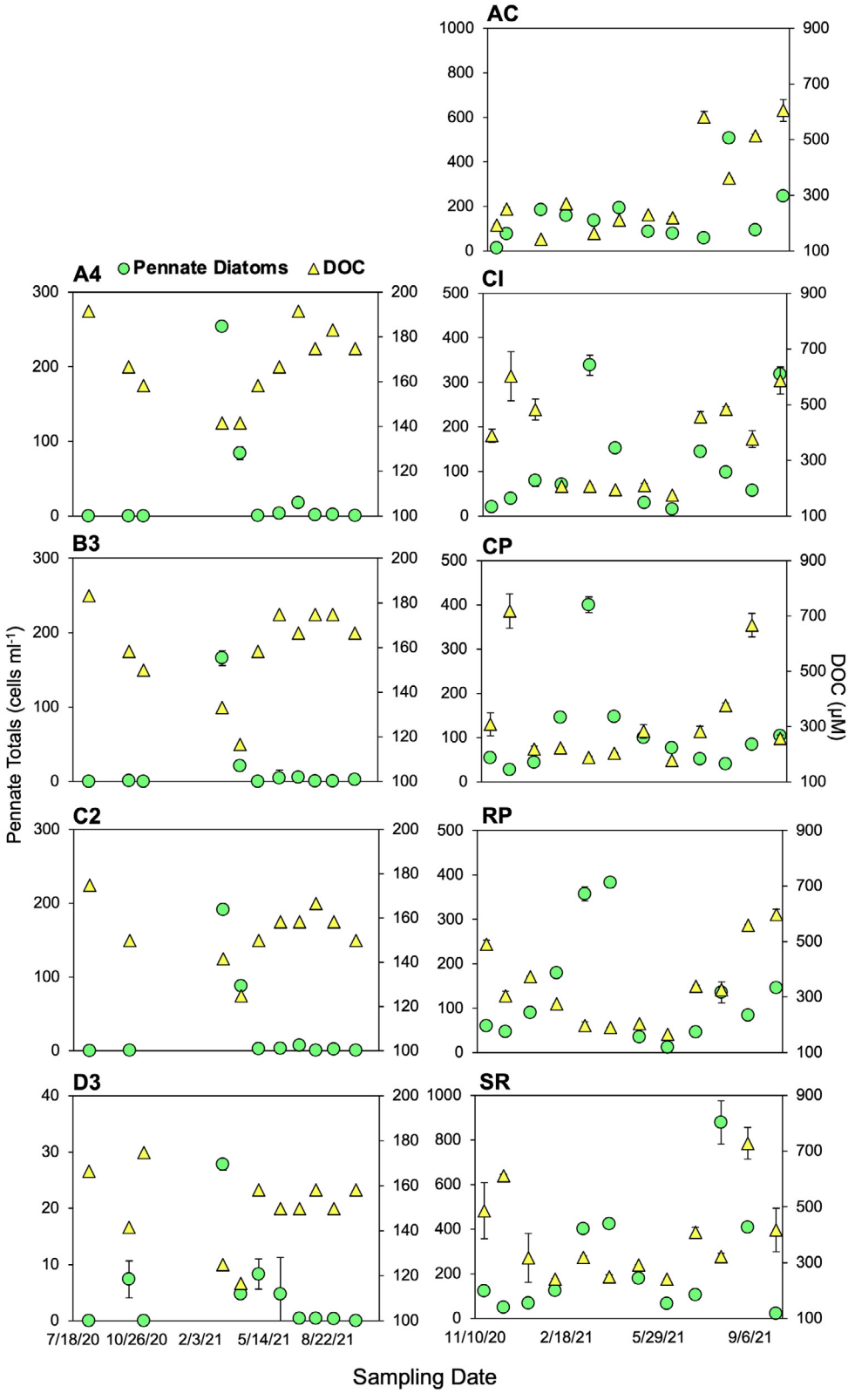

Fig. 6. Sum of mean (±SE) pennate diatom abundances and DOC concentrations summed per sampling date (given as mo/d/yr). Sites are labelled at the top-left corner of each panel (see Fig. 1 for explanation of site abbreviations). Markers cover error bars of some means. Note the difference in *y*-axis scales for pennate diatoms

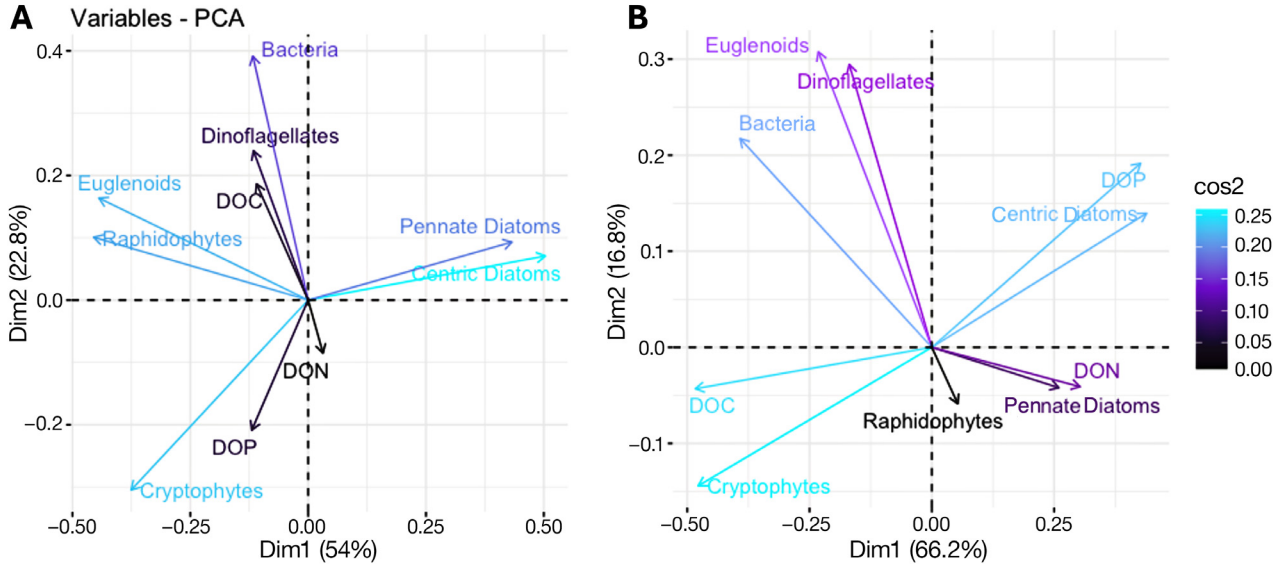

Fig. 7. Principal component analysis biplots for (A) mid-channel and (B) shore sites, depicting the impact of each variable on each principal component. Variables include abundances of major phytoplankton taxa (dinoflagellates, euglenoids, centric diatoms, pennate diatoms, raphidophytes, and cryptophytes), bacteria, and concentrations of dissolved organic nitrogen, phosphorus, and carbon (DON, DOP, and DOC)

DOC concentrations as diatom numbers decline (Fig. 6). Alternatively, DOC may inhibit pennate diatom growth, as bacteria have been shown to compete with diatoms for N uptake in the presence of sufficient DOC (Di Costanzo et al. 2023). Along the shore, sites closest to known point-source CSO N inputs, such as AC, had substantially higher DOM and both phytoplankton and bacterial abundances than other shore or mid-channel sites (Table S3). These observations contrast the general west-to-east mid-channel gradient of decreasing nutrient and microbial concentrations with distance from the NYC metropolitan area. Results underscore that not only are major phytoplankton taxa, particularly dinoflagellates, connected to bacterial populations but that localized terrestrial influences are important drivers of microbial ecological and biogeochemical processes in WLIS and presumably other developed coastlines.

4.2. Mid-channel versus shore sites

On average, WLIS shore waters were slightly fresher, presumably from riverine inputs, colder, more acidic, and had both lower DO and higher bacterial abundances than the mid-channel (Tables 1 & 2). Additionally, *T* across both regions depicted clear temporal trends of both phytoplankton and bacterial abundances, with diatom abundances peaking in the spring while dinoflagellates, euglenoids, and bacteria prevailed during summer (Fig. 4). This corresponded with summer maxima of chl *a* across all sites as previously reported in WLIS (Anderson & Taylor 2001, Rice & Stewart 2013, Liu et al. 2015, Roldan-Ayala et al. 2023, Brown et al. 2024).

The higher abundances of bacteria, phytoplankton, and concentrations of DOM (particularly DOC and DON) during spring and summer along the shore compared to the mid-channel were especially apparent at Site AC, where DOM levels and both phytoplankton and bacterial abundances were elevated (Figs. 4 & 5, Fig. S1). Site AC receives wastewater inputs from multiple point sources (5 CSOs; Fig. 1) and has been found to be highly enriched by DIN, notably NH_3 + NH_4^+ (an indicator of wastewater), in addition to nitrite + nitrate (NO_2^- + NO_3^-) (Brown et al. 2024). Site AC is also heavily influenced by wetland DOM inputs (Menendez & Tzortziou 2024).

Bacterial abundances were also more closely linked to total and <5 µm chl *a* levels at shore sites pooled than the mid-channel, with bacterial–chl *a* associations across all size fractions especially apparent at Site SR (consistent with the lowest salinity due to its location at the Saugatuck River mouth), despite no clear association between bacteria and individual phytoplankton taxa at this site (Table S1). Considering the proximity of Site SR to WTPs, and that riverine biological processing of DOM is mainly performed by heterotrophic bacteria (growth being dependent on DOM source) (Berggren & Del Giorgio 2015), it is

likely that the observed bacteria–chl *a* association was driven by high riverain DOM concentrations and/or autochthonous DOM production (Parr et al. 2015). The relative importance of either mechanism at Site SR is currently unknown.

Shore sites generally had a higher contribution of the <5 µm cell size fraction (presumably cyanobacteria) to not only overall chl *a* (Brown et al. 2024) but also relative to mid-channel sites (Roldan-Ayala et al. 2023) (Table S2). DAPI staining does not distinguish autotrophic versus heterotrophic cells. Therefore, the strong <5 µm cell size chl *a* and bacterial correlations across most sites could be accentuated by counts of smaller cyanobacteria that fell within the size range used to quantify bacterial abundances. The nanoplankton (5–20 µm) association with bacterial abundances found at only Sites SR and CI was most likely driven by bacterial–dinoflagellate correlations seen across both site regions (Table S1).

4.3. Nutrient and DOM enrichment in WLIS

Throughout this study, DOM levels corresponded to key phytoplankton taxa across both regions. For example, while DOC concentrations were typically positively associated with dinoflagellates, they were overwhelmingly negatively associated with pennate and centric diatoms (Table S1). LIS is generally a significant source of organic carbon (OC) to the Mid-Atlantic Bight, with summer (August) OC fluxes equating to 41×10^6 kg C mo^{-1} during low flow years due to net import of DOC (and export of particulate OC), and 30×10^6 kg C mo^{-1} during average flow years (Byrd et al. 2020). Thus, OC fluxes with greater net import into LIS could support higher phytoplankton abundances. In the nearby Great South Bay and Peconic Bays of Long Island, NY, elevated DOM (DON and DOC) concentrations were found to indirectly support higher nanoflagellate (primarily heterotrophic) biomass, with DOC positively associated with the <10 µm chl *a* cell size fraction (Lonsdale et al. 2006). Lastly, considering that summer DON concentrations were highest during peak *Prorocentrum* abundances in the mid-channel (Fig. S1), there is potential for DOM to fuel phytoplankton blooms in WLIS.

Proximity to NYC was an additional factor as both Site A4 (mid-channel) and Site CI (shore) are near the East River–WLIS confluence and characterized by above-average concentrations of DOC and bacterial cells. This is consistent with prior research showing elevated TN, delivered partially from the East River to WLIS, compared to central and eastern LIS (Vaudrey 2017, Vlahos & Whitney 2017, Vlahos et al. 2020). Approximately 700 CSO and 44 sewage treatment plant facilities discharge N-rich wastewater into the estuary (NYCDEP 2023). The WLIS flow exchange with the East River tidal strait is 10 times greater than the total net TN import into WLIS, with 32×10^6 kg N yr^{-1} from incoming river exchange fluxes (Vlahos et al. 2020). The high TN loading in the westernmost portion underscores the significant role played by N cycling into and from the East River, where most NYC wastewater inputs originate (Vlahos et al. 2020). In addition, the shore sites in closest proximity to point-source wastewater inputs, Sites AC and SR, had higher DON than the other shore sites, indicating terrestrial loading (Fig. S1). Sewage treatment plants generally release ~79×10^2 kg N d^{-1} to LIS as of 2022 (Long Island Sound Study 2023). Site AC, which depicted the highest DOM and microbial levels compared to the other sites (Figs. 4 & 5), is influenced by localized inputs and/or biogeochemical cycling processes that regulate DIN availability (Brown et al. 2024), presumably driving heightened phytoplankton and/or microbial abundances and *in situ* DOM production.

N forms (particularly DIN) help to regulate LIS phytoplankton biomass and community composition (Brown et al. 2024). Results from nutrient addition bioassays showed NO_2^- + NO_3^- increased diatom abundances, whereas euglenoids, cryptophytes, and dinoflagellates exhibited a preference for NH_3 + NH_4^+ (Brown et al. 2024). Considering that diatom abundances were dominant in the spring, followed by dinoflagellate and euglenoid abundances in the summer and fall during this study (Fig. 4), it is likely that the DIN form and *T* combined substantially influenced WLIS phytoplankton community composition. Other studies have explored linkages between dissolved forms of N and LIS phytoplankton species abundances and community composition (Anderson & Taylor 2001, Gobler et al. 2006, Suter et al. 2014, Roldan-Ayala et al. 2023). In the present study, despite DON showing few direct significant correlations with phytoplankton taxa and biomass (Table S1), overall N loading could propel significantly higher shore abundances and enhance dinoflagellate blooms.

4.4. Phytoplankton–bacterial associations

The overwhelming positive association between dinoflagellate and bacterial abundances (Table S1, Fig. 2), combined with the positive and often significant correlation between dinoflagellates and DOC

(Table S1), suggests that dinoflagellate-generated DOC may be a critical DOM substrate for WLIS bacterial production. While correlation does not necessarily mean causation, DOM exudation, particularly DOC by diatoms (Amin et al. 2012) or dinoflagellates (Oh et al. 2018), can be a significant resource for heterotrophic bacterial populations in marine environments (Amin et al. 2012). In LIS, Vlahos & Whitney (2017) found that with river inputs (flow rate) of >26 kg^3 yr^{-1}, LIS becomes an exporter of DOC and net autotrophic, showing that DOC quality is enriched by *in situ* primary production. Moreover, net DOC export contributes more to the annual decrease in WLIS DOC mass storage (-2.2×10^6 kg yr^{-1}) than other LIS regions, resulting in a net *in situ* DOC loss through processes such as heterotrophic bacterial respiration as well as burial of 1.4×10^6 kg yr^{-1} (Vlahos & Whitney 2017).

In laboratory culture studies, bacterial concentrations have been found to positively correlate with dinoflagellate cell abundances during exponential growth, indicating that bacterial production can become limited by dinoflagellate-derived C (Bolch et al. 2017), which would explain the positive dinoflagellate–bacterial relationship observed herein. Dinoflagellate DOM exudation varies by both taxa and cell size (López-Sandoval et al. 2013). For example, *Prorocentrum*, one of the dominant WLIS genera, can release protein-like fluorescent DOM (Romera-Castillo et al. 2010). The quality and quantity of autochthonous DOM release may therefore influence dinoflagellate–bacterial associations. Other studies have found similar associations, as dinoflagellate abundances were significantly correlated with pathogenic *Vibrio vulnificus* and *V. parahaemolyticus* levels in South Carolina coastal stormwater ponds, likely from dinoflagellate-produced DOC providing a suitable particle attachment matrix for *Vibrio*s (Greenfield et al. 2017).

WLIS dinoflagellate and bacterial populations may also be impacted, at least partially, by mutualism and/or commensalism, similar to other phytoplankton–bacterial co-occurrences (Haines & Guillard 1974, Guo & Tong 2014, Sañudo-Wilhelmy et al. 2014, Nair et al. 2022). For example, culture studies have revealed that some bacteria within the dinoflagellate pychosphere produce essential vitamins and other organic substrates (Tang et al. 2010, Cruz-López & Maske 2016, Cruz-López et al. 2018) such that affiliated dinoflagellate species are unable to grow axenically (Steidinger 2009, Bolch et al. 2011). Additionally, certain bacterial taxa enhance both the growth rates and/or toxicity of harmful algal bloom (HAB) dinoflagellates (Wang et al. 2018), positively correlate with toxin concentrations (Wu et al. 2022), and have been suspected of producing, modifying, or generally influencing some dinoflagellate toxin concentrations and intracellular toxin production (Maas et al. 2007, Albinsson et al. 2014, Tarazona-Janampa et al. 2020). It may also be possible for phycotoxins themselves to act as bacterial nutrients, as seen during a toxic bloom of the diatom *Pseudo-nitzschia* (Sison-Mangus et al. 2016). Thus, the connection between bacterial abundances and harmful phytoplankton should be further investigated in WLIS, especially considering that blooms of the HAB dinoflagellate species *Margalefidinium polykrikoides* have been found to co-occur with significantly higher heterotrophic bacteria levels than those outside blooms in Great South Bay and the Peconic Bays (Koch et al. 2014).

Exceptions to the tight dinoflagellate–bacteria population synergies occurred at the easternmost sampling sites for both mid-channel (Site D3) and shore (Site SR) regions, as neither site exhibited significant correlations between bacterial abundances and any evaluated phytoplankton taxon (Tables S1 & S4). Explanations could include hydrological factors, as Site D3 has a relatively greater exchange with the Atlantic Ocean and Site SR is presumably heavily influenced by the Saugatuck River flow.

Of dinoflagellates observed during this study, the genus *Prorocentrum* depicted the strongest positive relationships with bacterial abundances, with population levels generally coinciding with DOC concentrations (Table S4). Organic nutrients can provide a competitive advantage for dinoflagellates, such as *Prorocentrum* (e.g. Zhang et al. 2023). The phycosphere (microscale region rich in OM surrounding the phytoplankton cell; Bell & Mitchell 1972, Seymour et al. 2017) of *Prorocentrum* aggregates may in turn selectively favor certain bacteria (Tarazona-Janampa et al. 2020), as *Roseobacter* and *Marinobacter* clades have been associated with *P. cordatum* (Park et al. 2018). During this study, *P. lima*, *P. triestinum*, *P. cordatum*, and *P. micans* were detected at both WLIS shore and mid-channel sites, often reaching bloom levels (Roldan-Ayala et al. 2023, Brown et al. 2024) that coincided with elevated bacterial abundances. *Prorocentrum* can produce okadaic acid and other structurally related toxins associated with diarrheic shellfish poisoning (Beasley et al. 2023). This genus has been associated with fish kills across LIS regional estuaries such as the Peconic Bays, and it is a primary vernal bloom species in the nearby Great South Bay, Flanders Bay, and Moriches Bay, among others (Hattenrath-Lehmann & Gobler 2016, Tomar-

ken et al. 2016, Van Gulick 2021). Thus, understanding the composition and ecological function of bacteria associated with *Prorocentrum* will be useful for public safety and water quality management.

The positive relationship between abundances of the dinoflagellate *Heterocapsa* and bacteria at shore sites (Table S4) was unexpected because the genus can be bactivorous, typically having measurable bacterial ingestion rates (though *Heterocapsa* bactivory is low compared to other dinoflagellates; Seong et al. 2006). At Site AC, the site with elevated DON concentrations (Fig. S1), high *Heterocapsa* abundances coincided with greater summer bacterial abundances. These responses may be driven by organic N, as experimental studies have found that *H. rotundata* exhibits positive growth when urea is an available N source (Cira et al. 2016). Positive relationships between dinoflagellate and bacterial abundances exist in other urban US East Coast estuaries experiencing nutrient loading such as the Delaware Estuary (Kirchman et al. 2017) and Skidaway River Estuary (Anderson & Harvey 2022).

By comparison, the disconnect between diatom and bacterial abundances may have been influenced by DOC, particularly with pennate diatoms at mid-channel sites. Considering diatoms' increased contribution to the overall DOC pool under high-nutrient, low-light conditions (Bianchi et al. 2004, Thornton 2014), the increase in DOC following WLIS diatom blooms (Fig. 6) may be a product of leachate during cell senescence or cell lysis due to viral infection (Suttle 2005). Thus, the lag time between high diatom abundances and subsequent cell decay may explain the negative correlation between diatoms and bacterial abundances, notably the increased June bacterial abundances and DOC concentrations following diatom population declines (Fig. 6). In eastern LIS, Chen & Skoog (2021) found that as concentrations of some organic compounds decrease, bacterial abundances rose 50–476%, indicative of microbial degradation of biologically labile organic matter. Despite limited exploration of the associations between DOC and diatoms in urban estuaries, batch-culture bioassays conducted in coastal upwelling regions have shown that during the transition from a nutrient-replete to a nutrient-stressed state (particularly silica limitation), diatom-produced DOC became more bioavailable (Wear et al. 2015a,b) to bacteria. Investigating how diatoms use or generate DOC warrants further exploration because diatoms are often the numerically dominant taxon across LIS (Suter et al. 2014, Roldan-Ayala et al. 2023, Brown et al. 2024). Lastly, bacteria have been found to outcompete phytoplankton (diatoms specifically) for substrate uptake, particularly organic C (Znachor & Nedoma 2010), which could potentially generate a disconnect between the 2 populations.

5. CONCLUSIONS

This study revealed that dinoflagellate and bacterial abundances in WLIS are not only intricately associated, highlighting ecological interdependencies between the 2 clades, but that terrestrial inputs of nutrients may also drive higher concentrations of these populations. These findings highlight a novel aspect of WLIS estuarine microbial ecology and the importance of distinct phytoplankton taxa, rather than total biomass, in regulating phytoplankton–bacterial associations. Additionally, the study results imply that environmental conditions conducive to dinoflagellate population growth and DOC production may enhance bacterial populations (or bacteria alter dinoflagellate populations) in WLIS. The significantly higher microbial abundances at the shore compared to the mid-channel suggest that concentrations of nutrients (particularly DOM) from point-source wastewater inputs are primary drivers in the divergence of regions. Thus, urban inputs may alter microbial communities and localized biogeochemical cycling of DOM. These findings warrant assessments of how specific wastewater sources impact WLIS water quality, extending beyond the well-recognized cross-channel gradients (such as shore to mid-channel transects). Future research should explore ecological and biogeochemical interactions within and among phytoplankton and bacterial taxa, emphasizing molecular analyses that identify species- or group-specific associations with dinoflagellates. Moreover, the negative associations between pennate diatoms and DOC concentrations indicate that pennate diatoms are either using or inhibiting DOC production, potentially driving the lack of association between diatoms and bacteria. Together, these results underscore the importance of urban sources of nutrients in driving co-occurrences of phytoplankton taxa and bacteria as well as the potential for microbial communities to both influence and be impacted by DOM (primarily DOC) concentrations in WLIS and other urbanized estuarine systems.

Acknowledgements. We thank the crew of the RV 'John Dempsey' (CTDEEP) for assistance with water collection for mid-channel sites during their LIS surveys. We also thank Tzortziou laboratory members Dr. Maria Tzortziou, Kyle Turner, Dr. Jonathan Sherman, Dr. Minsun Lee, and Dr. Alana Menendez at the CUNY Center for Discovery and

Innovation for helping with sampling and logistics. We thank Tim Wahl at UWM for DOC analysis. Funding was courtesy of National Science Foundation award no. DEB-2039867, Environmental Protection Agency award no. LI 96261317 Subaward no. 82913/2/1156439, and startup funds awarded by the CUNY Advanced Science Research Center to D.I.G. Additionally, thank you for support from the CUNY Graduate Center Earth & Environmental Sciences Department, Dr. Stephen Arnott for statistical advice, and 3 anonymous reviewers who helped with the manuscript.

LITERATURE CITED

Ajani PA, Savela H, Kahlke T, Harrison D and others (2023) Response of planktonic microbial assemblages to disturbance in an urban sub-tropical estuary. Water Res 243: 120371

Albinsson ME, Negri AP, Blackburn SI, Bolch CJS (2014) Bacterial community affects toxin production by *Gymnodinium catenatum.* PLOS ONE 9:e104623

Amin SA, Parker MS, Armbrust EV (2012) Interactions between diatoms and bacteria. Microbiol Mol Biol Rev 76: 667–684

Anderson SR, Harvey EL (2022) Estuarine microbial networks and relationships vary between environmentally distinct communities. PeerJ 10:e14005

Anderson TH, Taylor GT (2001) Nutrient pulses, phytoplankton blooms, and seasonal hypoxia in the western Long Island Sound. Estuaries 24:228–243

Arandia-Gorostidi N, Krabberod AK, Logares R, Deutschmann IM and others (2022) Novel interactions between phytoplankton and bacteria shape microbial seasonal dynamics in coastal ocean waters. Front Mar Sci 9:901201

Arrieta JM, Herndl GI (2002) Changes in bacterial β-glucosidase diversity during a coastal phytoplankton bloom. Limnol Oceanogr 47:594–599

Asmala E, Haraguchi L, Markager S, Massicotte P, Riemann B, Staehr PA, Carstensen J (2018) Eutrophication leads to accumulation of recalcitrant autochthonous organic matter in coastal environment. Global Biogeochem Cycles 32:1673–1687

Beasley V, Carmichael W, Haschek WM, Golegrove KM, Solter P (2023) Phycotoxins. In: Haschek WM, Rousseaux CG, Wallig MA, Bolon B, Heinz-Taheny KM, Rudmann DG, Mahler BW (eds) Haschek and Rousseaux's handbook of toxicologic pathology, 4th edn, Vol 3. Academic Press, Cambridge, MA, p 305–391

Bell W, Mitchell R (1972) Chemotactic and growth responses of marine bacteria to algal extracellular products. Biol Bull 143:265–277

Berggren M, Del Giorgio PA (2015) Distinct patterns of microbial metabolism associated to riverine dissolved organic carbon of different source and quality. J Geophys Res Biogeosci 120:989–999

Bianchi TS, Filley T, Dria K, Hatcher PG (2004) Temporal variability in sources of dissolved organic carbon in the lower Mississippi River. Geochim Cosmochim Acta 68: 959–967

Bird DF, Karl DM (1999) Uncoupling of bacteria and phytoplankton during the austral spring bloom in Gerlache Strait, Antarctic Peninsula. Aquat Microb Ecol 19:13–27

Bolch CJS, Subramanian TA, Green DH (2011) The toxic dinoflagellate *Gymnodinium catenatum* (Dinophyceae) requires marine bacteria for growth. J Phycol 47:1009–1022

Bolch CJS, Bejoy TA, Green DH (2017) Bacterial associates modify growth dynamics of the dinoflagellate *Gymnodinium catenatum.* Front Microbiol 8:670

Brown M, Ambrosone M, Turner KJ, Humphries GE and others (2024) Phytoplankton assemblage responses to nitrogen following COVID-19 stay-in-place orders in western Long Island Sound (New York/Connecticut). Mar Environ Res 196:106371

Byrd AL, Vlahos P, Whitney MM, Menniti C, Warren JK (2020) Tidally resolved observations of organic carbon exchange through Eastern Long Island Sound. Estuar Coast Shelf Sci 232:106463

Chen TY, Skoog A (2021) Abiotic aggregation of organic matter in coastal and estuarine waters: cases in the Eastern Long Island Sound, USA. Water 13:3077

Cira EK, Paerl HW, Wetz MS (2016) Effects of nitrogen availability and form on phytoplankton growth in a eutrophied estuary (Neuse River Estuary, NC, USA). PLOS ONE 11:e0160663

Cruz-López R, Maske H (2016) The vitamin B_1 and B_{12} required by the marine dinoflagellate *Lingulodinium polyedrum* can be provided by its associated bacterial community in culture. Front Microbiol 7:560

Cruz-López R, Maske H, Yarimizu K, Holland NA (2018) The B-vitamin mutualism between the dinoflagellate *Lingulodinium polyedrum* and the bacterium *Dinoroseobacter shibae.* Front Mar Sci 5:274

CTDEEP (Connecticut Department of Energy and Environmental Protection) (2021) 2021 Long Island Sound hypoxia season review. CTDEEP, Hartford, CT

Di Costanzo F, Di Dato V, Romano G (2023) Diatom–bacteria interactions in the marine environment: complexity, heterogeneity, and potential for biotechnological applications. Microorganisms 11:2967

Ducklow HW (2000) Bacterial production and biomass in the oceans. In: Kirchman DL (ed) Microbial ecology of the oceans. John Wiley & Sons, New York, NY, p 85–120

Ducklow HW, Dickson A (1994) Determination of dissolved organic carbon by a high temperature combustion/direct injection technique. In: Knap A, Michaels A, Close A, Ducklow H, Dickson A (eds) Protocols for the joint global ocean flux study (JGOFS) core measurements. UNESCO–IOC, Paris, p 127–142

Fu H, Uchimiya M, Gore J, Moran MA (2020) Ecological drivers of bacterial community assembly in synthetic phycospheres. Proc Natl Acad Sci USA 117:3656–3662

Gay PS, O'Donnell J, Edwards CA (2004) Exchange between Long Island Sound and adjacent waters. J Geophys Res Oceans 109:C06017

Gobler CJ, Buck NJ, Sieracki ME, Sañudo-Wilhelmy SA (2006) Nitrogen and silicon limitation of phytoplankton communities across an urban estuary: the East River–Long Island Sound system. Estuar Coast Shelf Sci 68: 127–138

Graff JR, Rynearson TA (2011) Extraction method influences the recovery of phytoplankton pigments from natural assemblages. Limnol Oceanogr Methods 9:129–139

Grasshoff K, Ehrhardt M, Kremling K (1999) Methods of seawater analysis, 3rd edn. Wiley Verlag Chemie, Weinheim, p 159–228

Greenfield DI, Gooch Moore J, Stewart JR, Hilborn ED and others (2017) Temporal and environmental factors driving *Vibrio vulnificus* and *V. parahaemolyticus* populations and their associations with harmful algal blooms in South Carolina detention ponds and receiving tidal creeks. Geohealth 1:306–317

Grossart HP, Levold F, Allgaier M, Simon M, Brinkhoff T (2005) Marine diatom species harbour distinct bacterial communities. Environ Microbiol 7:860–873

Guo Z, Tong YW (2014) The interactions between *Chlorella vulgaris* and algal symbiotic bacteria under photoautotrophic and photoheterotrophic conditions. J Appl Phycol 26:1483–1492

Haines KC, Guillard RRL (1974) Growth of vitamin B_{12}-requiring marine diatoms in mixed laboratory cultures with vitamin B_{12}-producing marine bacteria. J Phycol 10: 245–252

Hattenrath-Lehmann TK, Gobler CJ (2016) Historical occurrence and current status of harmful algal blooms in Suffolk County, NY, USA. Stony Brook University School of Marine and Atmospheric Sciences, Stony Brook, NY

Heisler J, Glibert PM, Burkholder JM, Anderson DM and others (2008) Eutrophication and harmful algal blooms: a scientific consensus. Harmful Algae 8:3–13

Humphries GE, Espinosa JI, Ambrosone M, Roldan-Ayala Z, Tzortziou M, Goes JI, Greenfield DI (2023) Transitions in nitrogen and organic matter form and concentration correspond to bacterial population dynamics in a hypoxic urban estuary. Biogeochemistry 163:219–243

JGOFS (Joint Global Ocean Flux Study) (1996) Determination of dissolved organic carbon by a high temperature combustion/direct injection technique. In: Knap AA, Close MA, Ducklow H, Dickson A (eds) Protocols for the Joint Global Ocean Flux Study (JGOFS) Core Measurements, Chapter 16. JGOFS, , Woods Hole Oceanographic Institution, MA, p 127–142

Keller DP, Hood RR (2011) Modeling the seasonal autochthonous sources of dissolved organic carbon and nitrogen in the upper Chesapeake Bay. Ecol Modell 222: 1139–1162

Kirchman DL, Cottrel MT, DiTullio GR (2017) Shaping of bacterial community composition and diversity by phytoplankton and salinity in the Delaware Estuary, USA. Aquat Microb Ecol 78:93–106

Klindworth A, Mann AJ, Huang S, Wichels A and others (2014) Diversity and activity of marine bacterioplankton during a diatom bloom in the North Sea assessed by total RNA and pyrotag sequencing. Mar Genomics 18:185–192

Koch F, Burson A, Zhang Tang Y, Collier JL, Fisher NS, Sañudo-Wilhelmy S, Gobler CJ (2014) Alteration of plankton communities and biogeochemical cycles by harmful *Cochlodinium polykrikoides* (Dinophyceae) blooms. Harmful Algae 33:41–54

Larsson U, Hagström A (1979) Phytoplankton exudate release as an energy source for the growth of pelagic bacteria. Mar Biol 52:199–206

Latimer JS, Tedesco MA, Swanson RL, Yarish C, Stacey PE, Garza C (eds) (2014) Long Island Sound: prospects for the urban sea. Springer, New York, NY

LeGresley M, McDermott G (2010) Counting chamber methods for quantitative phytoplankton analysis — haemocytometer, Palmer-Maloney cell and Sedgewick-Rafter cell. In: Karlson B, Cusack C, Bresnan E (eds) Microscopic and molecular methods for quantitative phytoplankton analysis. Intergovernmental Oceanographic Commission Manuals and Guides 55. UNESCO, Paris, p 25–30

Li HM, Tang HJ, Shi XY, Zhang CS, Wang XL (2014) Increased nutrient loads from the Changjiang (Yangtze) River have led to increased harmful algal blooms. Harmful Algae 39:92–101

Liu L, Lwiza KMM, Taylor GT (2015) Importance of the bacterial dynamics in model simulations of seasonal hypoxia. Cont Shelf Res 105:1–17

Long Island Sound Study (2015) Geography, history, and health of the Sound. In: Long Island Sound comprehensive conservation and management plan 2015. https://longislandsoundstudy.net/wp-content/uploads/2015/09/CCMP_LowRes_Hyperlink_Section2.pdf

Long Island Sound Study (2023) Long Island Sound study, a partnership to restore and protect the Sound — nitrogen loading. https://longislandsoundstudy.net/ecosystem-target-indicators/nitrogen-loading/ (accessed 1 Nov 2023)

Lonsdale DJ, Greenfield DI, Hillebrand EM, Nuzzi R, Taylor GT (2006) Contrasting microplanktonic composition and food web structure in two coastal embayments (Long Island, NY, USA). J Plankton Res 28:891–905

López-Sandoval DC, Rodríguez-Ramos T, Cermeño P, Marañón E (2013) Exudation of organic carbon by marine phytoplankton dependence on taxon and cell size. Mar Ecol Prog Ser 477:53–60

Maas EW, Latter RM, Thiele J, Waite AM, Brooks HJL (2007) Effect of multiple antibiotic treatments on a paralytic shellfish toxin-producing culture of the dinoflagellate *Alexandrium minutum.* Aquat Microb Ecol 48:255–260

Maher D, Eyre BD (2011) Insights into estuarine benthic dissolved organic carbon (DOC) dynamics using δ^{13}C-DOC values, phospholipid fatty acids and dissolved organic nutrient fluxes. Geochim Cosmochim Acta 75: 1889–1902

Menendez A, Tzortziou A (2024) Driving factors of colored dissolved organic matter dynamics across a complex urbanized estuary. Sci Total Environ 921:171083

Morán XAG, Ducklow HW, Erickson M (2013) Carbon fluxes through estuarine bacteria reflect coupling with phytoplankton. Mar Ecol Prog Ser 489:75–85

Nair S, Zhang Z, Li H, Zhao H, Shen H, Kao SJ, Zhang Y (2022) Inherent tendency of *Synechococcus* and heterotrophic bacteria for mutualism on long-term coexistence despite environmental interference. Sci Adv 8:eabf4792

Nikon (2015) Nikon NIS-Elements AR (Advanced Research) user's guide (ver. 4.50). Laboratory Imaging, Praha

Nilsson C, Sundback K (1996) Amino acid uptake in natural microphytobenthic assemblages studied by microautoradiography. Hydrobiologia 332:119–129

NYCDEP (New York City Department of Environmental Protection) (2023) Combined sewer overflows. https://www.nyc.gov/site/dep/water/combined-sewer-overflows.page (accessed 23 Dec 2023)

Oh YH, Lee YW, Kim TH (2018) *In situ* production of dissolved organic carbon (DOC) by phytoplankton blooms (*Cochlodinium polykrikoides*) in the southern sea of Korea. J Sea Res 138:19–23

Park BS, Guo R, Lim WA, Jang SK (2018) Importance of free-living and particle-associated bacteria for the growth of the harmful dinoflagellate *Prorocentrum minimum*: evidence in culture stages. Mar Freshw Res 69:290–299

Parr TB, Cronan CS, Ohno T, Findlay SEG, Smith SMC, Simon KS (2015) Urbanization changes the composition and bioavailability of dissolved organic matter in headwater streams. Limnol Oceanogr 60:885–900

Porter K, Feig YS (1980) The use of DAPI for identifying and counting aquatic microflora. Limnol Oceanogr 25:943–948

Reed ML, DiTullio JR, Kacenas SE, Greenfield DI (2015) Effects of nitrogen and dissolved organic carbon on microplankton abundances in four coastal South Carolina systems. Aquat Microb Ecol 76:1–14

Rice E, Stewart G (2013) Analysis of interdecadal trends in chlorophyll and temperature in the Central Basin of Long Island Sound. Estuar Coast Shelf Sci 128:64–75

Riemann L, Steward GF, Azam F (2000) Dynamics of bacterial community composition and activity during a mesocosm diatom bloom. Appl Environ Microbiol 66:578–587

Roldan-Ayala Z, Arnott SA, Ambrosone M, Espinosa JI and others (2023) The influence of phenology, spatial distribution, and nitrogen forms for driving Long Island Sound phytoplankton biomass and community composition. Estuar Coast Shelf Sci 292:108451

Romera-Castillo C, Sarmento H, Alvarez-Salgado XA, Gasol JM, Marrasé C (2010) Production of chromophoric dissolved organic matter by marine phytoplankton. Limnol Oceanogr 55:446–454

Sañudo-Wilhelmy SA, Gómez-Consarnau L, Suffridge C, Webb EA (2014) The role of B vitamins in marine biogeochemistry. Annu Rev Mar Sci 6:339–367

Seong KA, Jeong HJ, Kim S, Kim GH, Kang JH (2006) Bacterivory by co-occurring red-tide algae, heterotrophic nanoflagellates, and ciliates. Mar Ecol Prog Ser 322:85–97

Seymour JR, Amin SA, Raina JB, Stocker R (2017) Zooming in on the phycosphere: the ecological interface for phytoplankton–bacteria relationships. Nat Microbiol 2: 17065

Sison-Mangus MP, Jiang S, Tran KN, Kudela RM (2014) Host-specific adaptation governs the interaction of the marine diatom, *Pseudo-nitzschia* and their microbiota. ISME J 8:63–76

Sison-Mangus MP, Jiang S, Kudela RM, Mehic S (2016) Phytoplankton-associated bacterial community composition and succession during toxic diatom bloom and non-bloom events. Front Microbiol 7:1433

Steidinger KA (2009) Historical perspective on *Karenia brevis* red tide research in the Gulf of Mexico. Harmful Algae 8:549–561

Strickland JDH, Parsons TR (1984) A practical handbook of seawater analysis, 2nd edn. Fisheries Research Board of Canada, Ottawa

Suter EA, Lwiza KMM, Rose JM, Gobler C, Taylor GT (2014) Phytoplankton assemblage changes during decadal decreases in nitrogen loadings to the urbanized Long Island Sound estuary, USA. Mar Ecol Prog Ser 497: 51–67

Suttle CA (2005) Viruses in the sea. Nature 437:356–361

Tamborski JJ, Cochran JK, Bokuniewicz HJ (2017) Submarine groundwater discharge driven nitrogen fluxes to Long Island Sound, NY: terrestrial vs. marine sources. Geochim Cosmochim Acta 218:40–57

Tang YZ, Koch F, Gobler CJ (2010) Most harmful algal bloom species are vitamin B_1 and B_{12} auxotrophs. Proc Natl Acad Sci USA 107:20756–20761

Tarazona-Janampa UI, Cembella AD, Pelayo-Zárate MC, Pajares S and others (2020) Associated bacteria and their effects on growth and toxigenicity of the dinoflagellate *Prorocentrum lima* species complex from epibenthic substrates along Mexican coasts. Front Mar Sci 7:569

Taylor GT, Way J, Yu Y, Scranton MI (2003) Ectohydrolase activity in surface waters of the Hudson River and western Long Island Sound estuaries. Mar Ecol Prog Ser 263: 1–15

Thermo Scientific (2010) Instructions. DAPI (4′, 6-diamidino-2′-phenylindole, dihydrochloride). Thermo Fisher Scientific, Rockford, IL

Thornton DCO (2014) Dissolved organic matter (DOM) release by phytoplankton in the contemporary and future ocean. Eur J Phycol 49:20–46

Tomarken JL, Gerstman M, Gobler CJ (2016) Investigation of fish kills occurring in the Peconic River–Riverhead, NY. Suffolk County Department of Health Services, New York, NY

Tuchman NC, Schollett MA, Rier ST, Geddes P (2006) Differential heterotrophic utilization of organic compounds by diatoms and bacteria under light and dark conditions. Hydrobiologia 561:167–177

Tucker S, Jones D, Lachat Application Group (2008a) Method 31-107-04-4-B: determination of total nitrogen in manual persulfate digests for seawater and brackish waters (low flow method). Lachat Instruments, Loveland, CO

Tucker S, Jones D, Lachat Application Group (2008b) Method 31-115-01-4-B: determination of total phosphorus in manual persulfate digests for seawater (low flow method). Lachat Instruments, Loveland, CO

Turner Designs (2017) Trilogy laboratory fluorometer user's manual version 1.5. Turner Designs, San Jose, CA

Van Gulick EV (2021) 2020 Connecticut harmful algal bloom report. State of Connecticut Department of Agriculture, Milford, CT

Van Patten P, O'Muin E, Moore M (2009) Sound facts — fun facts about Long Island Sound, 2nd edn. Connecticut Sea Grant, Groton, CT

Variem SS, Kizhakkedath VK (2021) Phycosphere associated bacteria; a prospective source of bioactive compounds. Biologia 76:1095–1098

Vaudrey J (2017) New York City's impact on Long Island Sound water quality. Technical report. University of Connecticut and Save the Sound, New Haven, CT

Verity PG, Borkman DG (2010) A decade of change in the Skidaway River Estuary. III. Plankton. Estuar Coast 33: 513–540

Vlahos P, Whitney MM (2017) Organic carbon patterns and budgets in the Long Island Sound estuary. Limnol Oceanogr 62:S46–S57

Vlahos P, Whitney MM, Menniti C, Mullaney JR, Morrison J, Jia Y (2020) Nitrogen budgets of the Long Island Sound estuary. Estuar Coast Shelf Sci 232:106493

Wang B, Yao M, Zhou J, Tan S and others (2018) Growth and toxin production of *Gambierdiscus* spp. can be regulated by quorum-sensing bacteria. Toxins 10:257

Wear EK, Carlson CA, James AK, Brzezinski MA, Windecker LA, Nelson CE (2015a) Synchronous shifts in dissolved organic carbon bioavailability and bacterial community responses over the course of an upwelling-driven phytoplankton bloom: bloom-induced shifts in DOC availability. Limnol Oceanogr 60:657–677

Wear EK, Carlson CA, Windecker LA, Brzezinski MA (2015b) Roles of diatom nutrient stress and species identity in determining the short- and long-term bioavailability of diatom exudates to bacterioplankton. Mar Chem 177:335–348

Welschmeyer N (1994) Fluorometric analysis of chlorophyll *a* in the presence of chlorophyll *b* and pheopigments. Limnol Oceanogr 39:1985–1992

Wu Z, Lee WH, Liu Z, Lin S, Lam PKS (2022) Microbiome associated with *Gambierdiscus balechii* cultures under different toxicity conditions. Front Mar Sci 9:760553

Zhang X, Zhen G, Cui X, Zeng Y, Gao W, Yu K, Li K (2023) Effect of dissolved organic nutrients on the bloom of *Prorocentrum donghaiense* in the East China Sea coastal waters. Mar Environ Res 183:105841

Znachor P, Nedoma J (2010) Importance of dissolved organic carbon for phytoplankton nutrition in a eutrophic reservoir. J Plankton Res 32:367–376

Editorial responsibility: Robert Sanders, Philadelphia, Pennsylvania, USA
Reviewed by: 3 anonymous referees

Submitted: December 31, 2023
Accepted: July 24, 2024
Proofs received from author(s): September 10, 2024